Analysis of Lamb Wave Excitation by the Partly Debonded Circular Piezoelectric Wafer Active Sensors

Mikhail V. GOLUB [1,*], Inka BUETHE [2], Alisa N. SHPAK [1],
Claus-Peter FRITZEN [2], Henning JUNG [2], Jochen MOLL[3]

[1] Institute for Mathematics, Mechanics and Informatics, Kuban State University; Krasnodar, Russia
E-mail: m_golub@inbox.ru, alisashpak7@gmail.com
[2] Institute of Mechanics and Control Engineering-Mechatronics, University of Siegen, Siegen, Germany
E-mail: inka.buethe@uni-siegen.de, claus-peter.fritzen@uni-siegen.de, henning.jung@uni-siegen.de
[3] Johann Wolfgang Goethe- Universität, D-60438 Frankfurt am Main, Germany
E-mail: moll@physik.uni-frankfurt.de

Abstract
The aim of the present work is the development of mathematical models for simulation and analysis of elastic waveguides with piezoelectric wafer active sensors (PWASs) generating Lamb waves, taking into account the partial debonding. The continuous wavelet transformation is applied to the recorded signal in order to identify the debonded part of the investigated PWAS. More specifically it is used to compute the carrier frequency of the generated wavefield which could significantly differ from the central frequency of the input signal especially in the case of a debonded PWAS. A carrier frequency shift both in the time and frequency domain in the case of debonded PWAS is to be observed due to potential non-linear contact effects such as coming from chattering. It was revealed that both carrier frequency shift and its time of arrival depend on the shape of the debonded part of the PWAS.

Keywords: piezoelectric wafer active sensor (PWAS), wavelet analysis, Lamb waves, integral approach

1. Introduction

Structural health monitoring (SHM) systems provide engineers with information about real-time structural conditions. Active health monitoring techniques that are based on Lamb waves often use a certain number of piezoelectric transducers. Evidently monitoring of the sensors serviceability is also necessary, and while totally debonded sensor can easily be detected, small debondings could still occur [1]. Such defects might lead to significant problems in the SHM system that might be more critical than total transducer failure, because the operator trusts in the sensor and the corresponding information about the health status of the structure.

The aim of the present work is continuation of the development of mathematical models [2,3,4] for simulation and analysis of elastic waveguides with piezoelectric wafer active sensors (PWASs) generating Lamb waves, taking into account the partial debonding and therefore accumulation of the knowledge about the effects and dynamics of partially debonded PWASs.

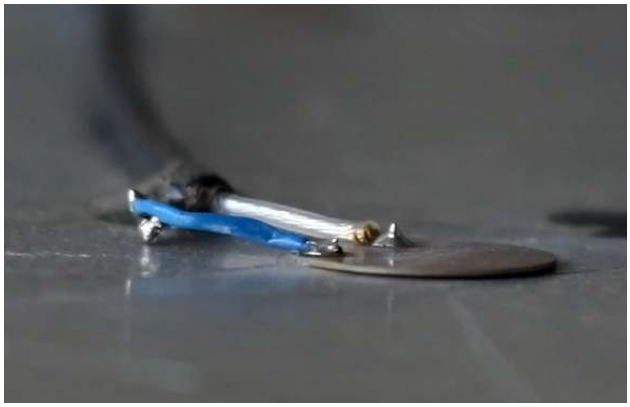

Figure 1 *– partially debonded PWAS*

Circular PWASs with disk-wrapped electrode are widely used in practical applications and therefore they are chosen as a subject of present research. In order to reveal the difference in the wavefield generated by the bonded and debonded actuators an experiment has been conducted. PWASs with various extent of debonding were attached to an aluminium plate and excited by a Hann-windowed toneburst voltage signal of certain central frequency from 30 kHz to 180 kHz. Generated velocities of the out-of-plane motion were measured with a laser vibrometer on the surface of the plate. For a certain sufficiently debonded PWAS some

interesting abnormalities were detected for high frequencies (e.g. 180 kHz). A sizable increase in the amplitude of the velocity of the motion was observed (up to 300 percent in comparison to perfectly bonded PWAS).

2. Statement of the problem

For the problem taken, two contacting media are considered. The underlying structure is made of isotropic elastic material (Aluminum), while the PWAS is of piezoelectric material [5]. The constitutive equations of the linear theory of piezoelasticity are as follows:

$$\sigma_{ij} = C_{ijkl} u_{k,l} - e_{kij} \varphi_{,k}, \quad D_i = e_{ikl} u_{k,l} + \in_{ik} V_{,k}.$$

They relate stress tensor σ_{ij}, displacements vector u_k, electric displacement vector D_i and electric potential V in terms of elastic moduli C_{ijkl}, piezoelectric e_{kij} and dielectric constants $\in_{ik}$. The comma in the subscript denotes derivative with respect to the corresponding Cartesian coordinate. The governing equations for the linear elasticity

$$\sigma_{ij,j} = \rho \frac{\partial^2 u_j}{\partial t^2}, \tag{1}$$

are completed by the electrostatic condition for piezoelastic case

$$D_{i,i} = 0.$$

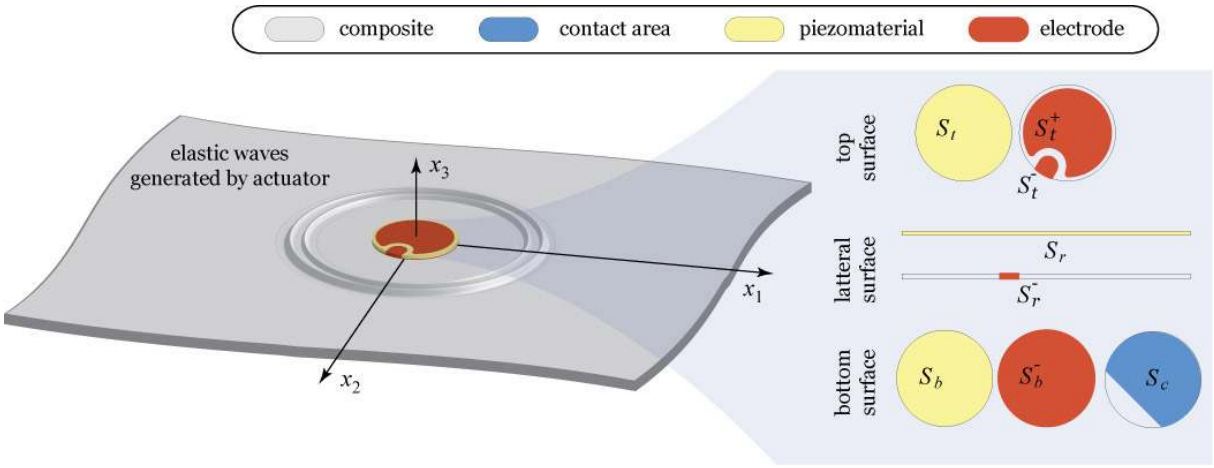

Figure 2 *– Geometry of the problem. Lamb wave excitation by the debonded PWAS.*

The Cartesian coordinates $\mathbf{x} = (x_1, x_2, x_3)$ are used in order to write a boundary value problem depicted in Figure 2. The layer occupies the domain $\Omega_1 = \{-H \le x_3 \le 0\}$; wavefields u_k^1 in this domain are denoted by superscript 1. The wavefields u_k^2 within the PWAS of thickness h_{PWAS} occupying the domain $\Omega_2 = \{0 \le x_3 \le h_{PWAS}, \sqrt{x_1^2 + x_2^2} \le R_{PWAS}\}$ are indicated by superscript 2; the subscripts are omitted below when the expressions are valid for the layer and the PWAS. The bottom surface of PWAS S_b and surface of contact between the PWAS and the layer S_c are different if the debonded PWAS is considered. Thus, the displacement vector is $\mathbf{u} = \mathbf{u}^1$ within the layer Ω_1 and $\mathbf{u} = \mathbf{u}^2$ within the PWAS domain Ω_2. The bonding or adhesive layer is not taken into account by the present model due to its small thickness.

The boundary conditions should be written carefully taking into account the geometry of the problem. The structure is at rest

$$\mathbf{u}(\mathbf{x}, t < 0) = 0, \quad \dot{\mathbf{u}}(\mathbf{x}, t < 0) = \frac{\partial \mathbf{u}(\mathbf{x}, t < 0)}{\partial t} = 0,$$

until the impulse function $p(t)$ is applied at the metallic electrode on surfaces of the PWAS

$$V(\mathbf{x},t) = V_0 p(t), \quad \mathbf{x} \in S_r^+,$$
$$V(\mathbf{x},t) = -V_0 p(t), \quad \mathbf{x} \in S_t^- \bigcup S_r^- \bigcup S_b^-.$$

The bottom and upper surfaces of the layer are stress-free

$$\sigma^1 \cdot \mathbf{n}_{x_3}(\mathbf{x},t) = 0, \quad \mathbf{x} \in \{x_3 = -H\}, \quad \sigma^1 \cdot \mathbf{n}_{x_3}(\mathbf{x},t) = 0, \quad \mathbf{x} \in \{x_3 = 0\} / S_c,$$
$$\sigma^2 \cdot \mathbf{n}_{x_3}(\mathbf{x},t) = 0, \quad \mathbf{x} \in S_b / S_c, \quad \sigma^2 \cdot \mathbf{n}_r(\mathbf{x},t) = 0, \quad \mathbf{x} \in S_r,$$
$$\sigma^2 \cdot \mathbf{n}_{x_3}(\mathbf{x},t) = 0, \quad \mathbf{x} \in \left\{ x_3 = h_{PWAS} \ \& \ \sqrt{x_1^2 + x_2^2} \le R_{PWAS} \right\},$$

except the area S_c of the perfect contact between the PWAS and the layer

$$\begin{matrix} \sigma^1(\mathbf{x},t) \cdot \mathbf{n}_{x_3} = \sigma^2(\mathbf{x},t) \cdot \mathbf{n}_{x_3} = \mathbf{q}(\mathbf{x},t) \\ \mathbf{u}^1(\mathbf{x},t) = \mathbf{u}^2(\mathbf{x},t) \end{matrix}, \quad \mathbf{x} \in S_c, \tag{2}$$

In order to understand dynamics of the coupled system (layer and the PWAS) mathematical description should be provided. The boundary-value problem defined above can be simplified if the Laplace transform is applied

$$\mathbf{u}(\mathbf{x},t) = \frac{1}{\pi} \mathrm{Re} \int_0^\infty \mathbf{U}(\mathbf{x},\omega) P(\omega) e^{-i\omega t} d\omega$$

Laplace transforms of the displacements (harmonic solution) in domains Ω_i are connected via equations (2). Wavefields in the layer can be represented as Fourier integrals [6]

$$\mathbf{U}^1(x_1,x_2,x_3,\omega) = \frac{1}{4\pi^2} \int_{-\infty}^{\infty} \int_{-\infty}^{\infty} \mathbf{K}(\alpha_1,\alpha_2,x_3,\omega) \mathbf{Q}(\alpha_1,\alpha_2,\omega) e^{i(x_1\alpha_1, + x_2\alpha_2)} d\alpha_1 d\alpha_2, \tag{3}$$

where $K(\alpha_1,\alpha_2,x_3,\omega)$ is the Fourier transform of Green's matrix and $\mathbf{Q}(\alpha_1,\alpha_2,\omega)$ is the Fourier transform of stresses $\mathbf{q}$ on the contact surface S_c. Due to the equality $\mathbf{U}^1 = \mathbf{U}^2$ in the Fourier space, the solution of the problem takes into account spectral properties of the layer (poles of $\mathbf{K}$), of the PWAS and points of the discrete spectrum of the coupled problem. The influence of these spectrums can be seen as normal modes or Lamb waves, eigenmodes of the PWAS (eigenfrequencies) and resonances induced by coupling between them.

3. Experiment

3.1 Experimental setup

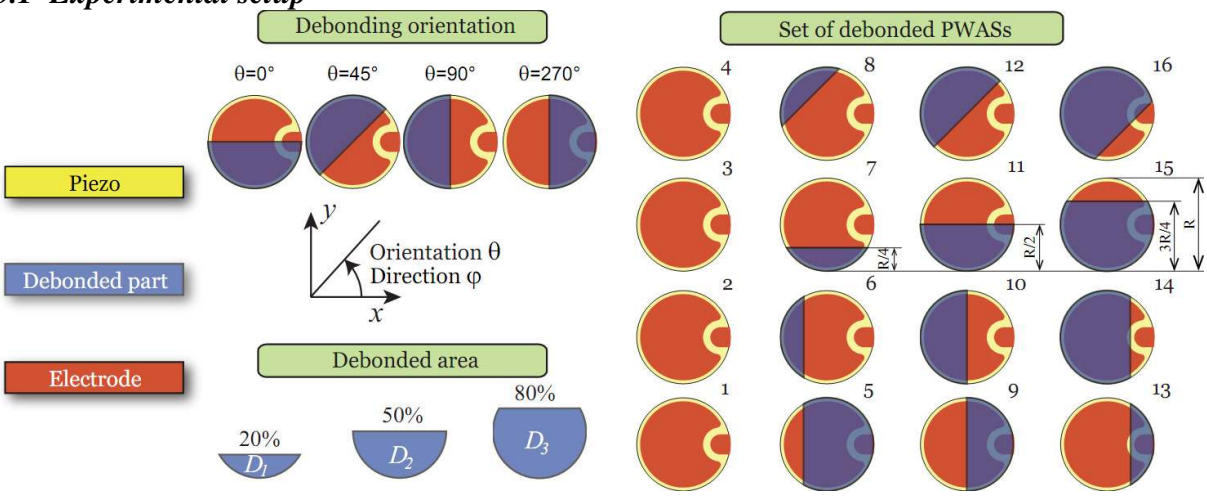

Figure 3 – Design of the specimen and the geometry of debondings

For the investigation of the effects of partially debonded PWASs and in order to reveal the difference in the wavefields, generated by the actuators of different attachment an experiment

has been performed. Sixteen PWASs of various extent of debonding have been glued to the surface of an aluminum plate of the dimensions 500 mm by 550 mm and a thickness of H = 2 mm. The orientation and the positions of soldering points of all the PWASs are the same way in order to neutralize the effect of wavefield directionality coming from PWAS orientation (see [3]). Variety of sizes and shapes of the debonded areas are shown in Fig. 3.
A Laser Doppler Vibrometer (LDV) is used to measure the velocities of the out-of-plane motion generated by the certain PWAS on the surface $z = H$ of the plate, see more details in [3]. Measurements for each PWAS are performed at the radius of 20 mm around the center of PWAS. A Hann-windowed toneburst voltage signal of a certain central frequency f_0 varying from 30 kHz to 180 kHz is used:

$$p(t) = \frac{1}{2}\cos(2\pi f_0 t)\left(1-\cos\left(\frac{2\pi f_0 t}{N}\right)\right), \quad 0 < t < \frac{N}{f_0}.$$

3.2 Data measured

All measurements were performed with $N = 5$, which is optimal for the frequency range considered [3]. For most cases the amplitudes generated by a debonded PWAS is much smaller compared to the perfectly glued one due to the smaller contact area with the plate. For some angles φ and frequencies the amplitudes are much greater for the debonded actuator in comparison with fully glued, e.g. at the central frequency $f_0 = 180$ kHz that is shown in Fig. 4. Such effects can be explained due to phenomenon of the standing waves in the range near resonance frequencies f_n where signal is trapped with the PWAS as in case of crack [4].

4. Analysis

4.1 Continuous Wavelet transform

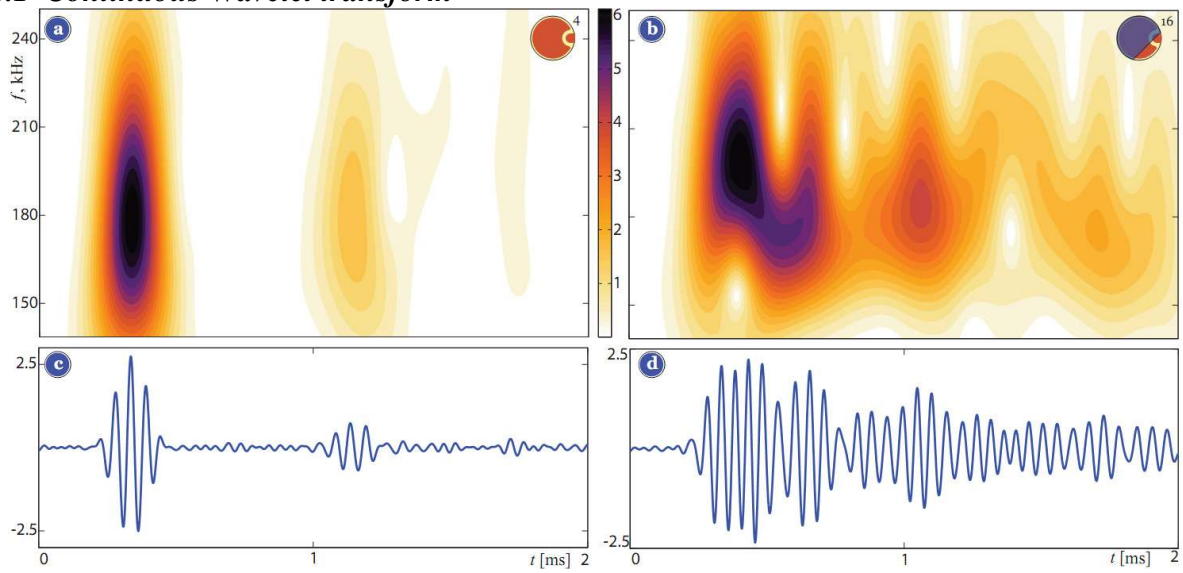

Figure 4 – Continuous Wavelet transform and A-scans for the direction $\varphi = 230°$, for perfectly bonded PWAS 4 (a, c) and strongly debonded PWAS 16 (b, d); central frequency $f_0 = 180$ kHz.

Time-frequency analysis is used to study resonance frequencies and the dynamics of the generated wavefield. For that purpose continuous wavelet transform has been accepted as an appropriate method as long as it allows analysing the signal spectrum at any point within the time-domain considered. Continuous wavelet transform is performed using the formula:

$$W(\omega,t) = \sqrt{\frac{\omega}{\omega_0}}\int_{t_1}^{t_2} u(\xi - t)\psi_G\left(\frac{(\xi - t)\omega}{\omega_0}\right)d\xi,$$

where $\psi_G(t)$ is kernel wavelet function, $u(\xi)$ is the recorded signal, $\xi \in [t_1, t_2]$ and $\omega_0 = 2\pi f_0 H / \mathrm{v}_{SV}$, f_0 is the central frequency of the input voltage signal and ω_0 is corresponding non-dimensional value. The Gabor wavelet with the factor $G = 0.5$ is selected as a kernel function due to its waveform is similar to the generated signal used in the experiment (see more in [7]):

$$\psi_{Gabor}(t) = \pi^{0.25}(\omega_0 / \gamma)^{0.5} \exp\left(-0.5G(\omega_0 t / \gamma)^2 + \mathrm{i}\,\omega_0 t\right), \quad \gamma = \pi\sqrt{2/\ln 2}$$

Results of the wavelet transform are shown in Figure 4 for two PWASs, along with the A-scans. The difference both in the spectrum and in the registered signal is to be observed.

4.2 Carrier and instantaneous frequencies

Continuous wavelet transform permits to compute the carrier frequency f_c of the generated wavefield which could significantly differ from the central frequency f_0 of the input signal especially in the case of a debonded PWAS because of resonance frequencies related to the coupling effect. Carrier frequency of the recorded signal $u(t)$ and its time of arrival t_a are defined from the maximum of the absolute value of the wavelet transform $W(f_c, t_a) = \max|W(\omega, t)|$. Instantaneous frequencies (IF) can be also computed from the measured signal [8]:

$$\tilde{\omega}(\omega^*, t^*) = \frac{1}{2\pi}\mathrm{Im}\left[\frac{1}{W(\omega^*, t^*)}\frac{dW(\omega^*, t^*)}{dt}\right],$$

where ω^* is non-dimensional value corresponding to the frequency used in the maximum of the wavelet transform with the fixed t^*:

$$W(\omega^*, t^*) = \max|W(\omega, t^*)|.$$

Here $\tilde{\omega}$ is non-dimensional instantaneous frequency computed for the fixed time t^* ($\tilde{\omega} = 2\pi\tilde{f}H / \mathrm{v}_{SV}$). IFs are shown in the Figure 5 put on the wavelet transform plot $|W(\omega, t)|$. The carrier frequency almost coincides with IF at the moment t_a. IFs can be used as well as carrier frequencies, IFs provide information in time domain. It might be useful in the case of detailed analysis in conjunction with full mathematical description. IFs may reveal the debonding of the PWAS: the variation of IF in time domain depends on the scatter/source [8]. Thus, information on resonance and eigen-frequencies can be excluded from the measured data using wavelet analysis and IFs.

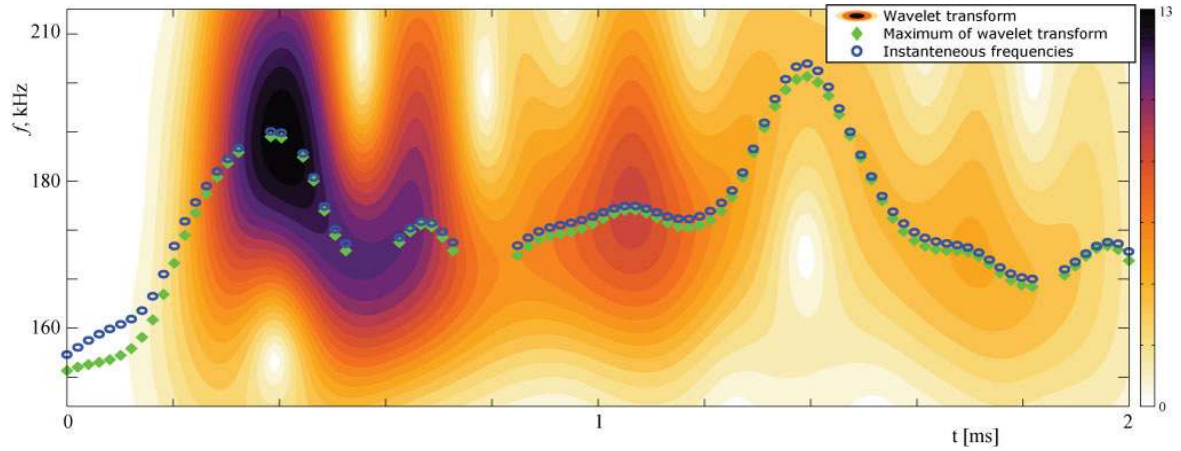

Figure 5 – Wavelet transform and instantaneous frequencies for the direction ϕ = 230°, for PWAS 16 with central frequency $f_0 = 180\,kHz$.

4.3 Numerical analysis

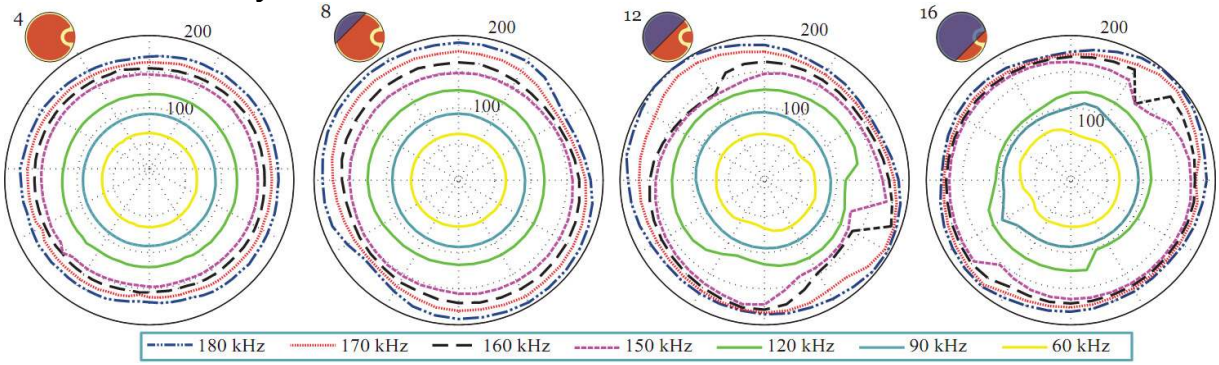

Figure 6 – Carrier frequencies of the generated wavefield

Figure 6 shows carrier frequencies computed for each measurement. A difference between carrier and central frequency for debonded actuator is to be observed. Moreover, this difference increases and shifts to the resonance frequencies f_n with the decrease of the contact area S_c.

Figure 7 shows time of arrival of the carrier frequency in case of debonded PWASs with different debonded area orientation ($\theta = 0^o, 45^o, 180^o$) in comparison with the same measurements for the perfectly glued PWAS. Time of arrival of the package with carrier frequency increases with the growth of the central frequency for debonded actuators, at the same time in case of perfectly capacitive PWAS time of arrival decreases with the growth of the central frequency.

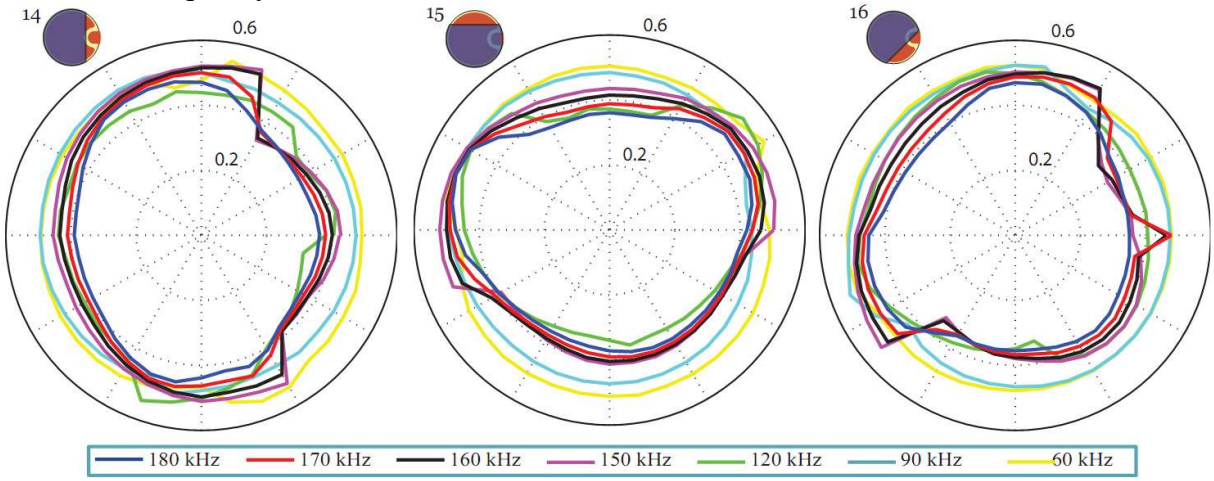

Figure 7 – Time of arrival of the carrier frequency in case of debonded PWASs with the debonded area orientation D_3 ($\theta = 0^o, 45^o, 180^o$) in comparison with perfectly glued PWAS 4

From figures 4, 6, 7 it is possible to say that both carrier frequency and its time of arrival depend on the shape of the debonding. Theoretically these characteristics and resonance frequencies f_n can be used in order to identify the debonding, its shape and location. A validation is the subject of the future investigations.

5. Conclusion

To gain more knowledge about cirqular piezoactuators with various debondings, experiments have been conducted and analyzed. Continuous wavelet transform is applied to the recorded signal in order to compute the carrier and instantaneous frequencies and time of arrival of the

corresponding wave packages in the generated wavefield. A certain difference between central and carrier/instantaneous frequencies has been revealed, which is dependant on the shape of debonding. Certain shift in the time of arrival of the carrier frequency in case of the debonded actuator is observed, which also depends on the shape of debonding. The knowledge obtained about the dynamics of the debonded PWASs can be used in the field of structural health monitoring of the circular piezoactuators.

Acknowledgements

The work is supported by the Russian Foundation for Basic Research (Projects 12-01-33011 and 13-01-96516).

References

1. N P Yelve, M Mitra, and P M Mujumdar, "Higher harmonics induced in lamb wave due to partial debonding of piezoelectric wafer transducers," NDT & E International, vol. 63, pp. 21–27, Apr. 2014.
2. M V Golub, A N Shpak, I Buethe, C-P Fritzen, H Jung and J Moll, 'Continuous wavelet transform application in diagnostics of piezoelectric wafer active sensors' Proceedings of the International conference DAYS on DIFRACTION 2013, Saint-Petersburg, May 27–31, pp. 59-64, 2013.
3. J Moll, M V Golub, E Glushkov, N Glushkova and C-P Fritzen 'Non-axisymmetric Lamb Wave Excitation by Piezoelectric Wafer Active Sensors', Sensors and Actuators: A. Physical, Vol. 130, pp 113-121, 2012.
4. E Glushkov, N Glushkova, M Golub, J Moll and C-P Fritzen, 'Wave energy trapping and localization in a plate with a delamination', Smart Materials and Structures, Vol 21, 125001, 2012.
5. P Gaudenzi, Smart Structures: "Physical behavior, mathematical modeling and applications", A John Wiley and Sons, Ltd., Publication, 177 p., 2009.
6. E V Glushkov and N V Glushkova, 'On the efficient implementation of the integral equation method in elastodynamics', Journal of Computational Acoustics, Vol 9(3), pp 889-898, 2001.
7. K Kishimoto, H Inoue, M Hamada and T Shibuya, 'Time Frequency Analysis of Dispersive Waves by Means of Wavelet Transform', Journal of Applied Mechanics, Vol 62, pp 841–846, 1995.
8. O Nemytova, A Rinkevich and D Perov. 'Instantaneous frequency estimation used for the classification of echo signals from different reflectors', Russian Journal of Nondestructive Testing, Vol 48, pp 649-661, 2012.